# Structural Alignment of the (+)-*trans-anti*-Benzo[*a*]pyrene-dG Adduct Positioned Opposite dC at a DNA Template−Primer Junction†

Binbin Feng,‡ Andrey Gorin,‡ Brian E. Hingerty,§,|| Nicholas E. Geacintov,⊥ Suse Broyde,▽ and Dinshaw J. Patel*,‡

*Cellular Biochemistry and Biophysics Program, Memorial Sloan Kettering Cancer Center, New York, New York 10021, Oak Ridge National Laboratory, Oak Ridge, Tennessee 37831, Knox Computer Consultants, Knoxville, Tennessee 37923, and Chemistry and Biology Departments, New York University, New York, New York 10003*

*Received January 13, 1997; Revised Manuscript Received August 28, 1997*⊗

ABSTRACT: This study reports on the solution conformation of the covalent (+)-*trans-anti*-[BP]dG adduct (derived from the binding of the highly mutagenic and tumorigenic (+)-*anti*-benzo[*a*]pyrene diol epoxide to the $N^2$ of deoxyguanosine) positioned opposite dC at a junctional site in the d(A1-A2-C3-[BP]G4-C5-T6-A7-C8-C9-A10-T11-C12-C13)·d(G14-G15-A16-T17-G18-G19-T20-A21-G22-C23) 13/10-mer DNA sequence. The 13-mer represents the template strand containing the junction [BP]dG4 lesion while the complementary 10-mer models a primer strand which extends upto and is complementary to the modified dG4 residue. The solution conformation has been determined by initially incorporating intramolecular and intermolecular proton−proton distances defined by lower and upper bounds deduced from NOESY spectra as restraints in molecular mechanics computations in torsion angle space and subsequently through restrained molecular dynamics calculations based on a NOE distance and intensity refinement protocol. The duplex segment retains a minimally perturbed B-DNA conformation with all base pairs, including the junctional [BP]dG4·dC23 pair, in Watson−Crick hydrogen-bonded alignments. The pyrenyl ring is not stacked over the adjacent dC5·dG22 base pair but is positioned on the minor groove-side of the [BP]dG moiety and directed toward the 5′-end of the template strand. The pyrenyl ring stacks over the base of the non-adjacent dA2 residue in one direction and the sugar ring of dC23 in the other direction. The solution structure of the (+)-*trans-anti*-[BP]dG adduct opposite dC in the 13/10-mer in which the modified deoxyguanosine adopts an *anti* glycosidic torsion angle (this study) is in striking contrast to the structure of the same (+)-*trans-anti*-[BP]dG moiety in a 13/9-mer of the same sequence but without the dC23 residue positioned opposite the adduct site [Cosman, M., et al. (1995) *Biochemistry 34*, 15334−15350]. For the latter case, the aromatic portion of the BP residue stacks over the adjacent dC5·dG22 base pair, the modified deoxyguanosine adopts a *syn* glycosidic torsion angle and is displaced toward the major groove direction. Insights into the factors that affect the sequence and context dependent conformations of stereoisomeric [BP]dG lesions have emerged following comparison of these two structures with the minor groove conformations of the same (+)-*trans-anti*-[BP]dG lesion in the fully complementary 11-mer duplex [Cosman, M., et al. (1992) *Proc. Natl. Acad. Sci. U.S.A. 89*, 1914−1918] and in the base displaced-intercalative conformation of the 11/10-mer deletion duplex containing a −1 deletion site opposite the lesion [Cosman, M., et al. (1994) *Biochemistry 33*, 11507−11517]. The contributing factors where applicable include Watson−Crick base pairing at the site of the lesion, positioning of the carcinogen within the floor of the minor groove, and the tendency of the bulky hydrophobic aromatic BP residue to assume stacked or intercalative conformations.

The presence of bulky polycyclic aromatic residues derived from the binding of stereoisomeric mutagenic and tumorigenic metabolites of benzo[*a*]pyrene to deoxyguanosine residues in DNA, is known to block replication (Reardon et al., 1989; Hruszkewycz et al., 1992; Shibutani et al., 1993), to induce mutations (Wei et al., 1991; Rodriguez & Loechler, 1993), and is believed to constitute the critical intial step in carcinogenesis (Greenblatt et al., 1994; Ross et al., 1995; Denissenko et al., 1996). The most tumorigenic metabolite of the environmental pollutant benzo[*a*]pyrene (BP) is the (+)-7*R*,*8S*-dihydroxy-*9S*,*10R*-epoxy-7,8,9,10-tetrahydrobenzo[*a*]pyrene [(+)-*anti*-BPDE] [see reviews by Singer and Grunberger (1983) and Harvey (1991)]. The major adduct resulting from the reaction of (+)-*anti*-BPDE with native DNA involves the nucleophilic *trans*-addition of the exocyclic amino group of dG residues to $C^{10}$ of BPDE. The resulting (+)-*trans-anti*-[BP]dG moiety has been site-specifically incorporated into oligodeoxyribonucleotides of defined sequence for structural studies by NMR methods (Cosman et al., 1992, 1994, 1995; Fountain & Krugh, 1995), by optical spectroscopic techniques (Geacintov et al., 1991; Suh et al., 1995; Pontén et al., 1994), as well as for site-specific mutagenesis experiments *in vivo* (Mackay et al., 1992; Jelinsky et al., 1995; Moriya et al., 1996).

† This research is supported by NIH Grant CA-46533 to D.J.P., by NIH Grant CA-20851 and DOE Grant DE-FG02-88ER60405 to N.E.G., by NIH Grant CA-28038, NIH Grant RR-06458, and DOE Grant DE-FG02-90ER60931 to S.B., and by DOE Contract DE-AC05-840R21400 with Martin-Marietta Energy Systems and DOE OHER Field Work Proposal ERKP931 to B.E.H.

* Corresponding author.
‡ Memorial Sloan Kettering Cancer Center.
§ Oak Ridge National Laboratory.
|| Knox Computer Consultants.
⊥ Chemistry Department, NYU.
▽ Biology Department, NYU.

⊗ Abstract published in *Advance ACS Abstracts,* November 1, 1997.

S0006-2960(97)00069-X CCC: $14.00 

The conformations of stereoisomeric *anti*-[BP]dG lesions are remarkably dependent on the absolute configurations of substituents about the chiral $C^7$, $C^8$, $C^9$, and $C^{10}$ carbon atoms of the benzylic ring. In adducts with (+)-*trans-anti*- and (−)-*trans-anti*-[BP]dG lesions in the d(C-[BP]G-C)·d(G-C-G) sequence context at the 11-mer duplex level, the bulky pyrenyl residues are positioned in the minor grooves of intact B-DNA duplexes either toward the 5′-side or the 3′-side of the modified deoxyguanosyl residues, respectively (Cosman et al., 1992; de los Santos, 1992). However, in the stereoisomeric adducts with (+)-*cis-anti*- and (−)-*cis-anti*-adduct stereochemistry in the same sequence context, the pyrenyl residues are intercalated between adjacent dG·dC base pairs, with the modified deoxyguanosyl and partner dC residues displaced into opposite grooves of otherwise intact B-DNA duplexes (Cosman et al., 1993, 1996).

The local base sequence can also have a dramatic effect on the conformations of the (+)-*trans-anti*-[BP]dG moieties. In the deletion duplex containing the d(C-[BP]G-C)·d(G-G) sequence context at the 11/10-mer level (the partner base dC opposite the modified [BP]dG residue is missing), the pyrenyl residue is intercalatively inserted into the duplex with the modified deoxyguanosyl residue displaced into the major groove (Cosman et al., 1994). At a single strand−double strand 13/9-mer junction containing the d(A-A-C-[BP]-G-C---)·d(---G) sequence context that partially mimics the structure of a template−primer junction as it might exist in a complex with a polymerase (the base complementary to [BP]dG is missing), the pyrenyl residue stacks with the junctional dG·dC base pair and the glycosidic torsion angle of the [BP]dG residue is *syn* and the modified guanine is displaced into the groove (Cosman et al., 1995). Thus, the (+)-*trans-anti*-[BP]dG moieties assume strikingly different, local sequence-dependent conformations in the 11-mer duplex containing dC opposite the [BP]dG adduct, the 11/10-mer containing a deletion site opposite the [BP]dG adduct and the 13/9-mer template−primer junction with no base opposite the junctional [BP]dG adduct.

A detailed analysis of the conformational features of these and other related adducts suggests that several different, interdependent factors, play important roles in determining the conformations of *anti*-[BP]dG moieties in an oligonucleotide environment (Geacintov et al., 1997). These factors include (1) stereochemistry-dependent van der Waals steric hindrance effects between the covalently linked BP and dG residues, as well as with other nearby DNA residues, (2) the preference for stacking interactions between the hydrophobic pyrenyl residues and DNA bases and (3) the maintenance of Watson−Crick hydrogen bonding at the site of the lesion whenever possible. In the present work, the solution structure of the (+)-*trans-anti*-[BP]dG moiety (Figure 1A) in a 13/10-mer sequence context (Figure 1B) was explored to determine the effect of the complementary dC base opposite the lesion on its conformation. This template−primer junction is identical to the adduct 13/9-mer sequence studied previously (Cosman et al., 1995), except that the primer strand is now extended by one single complementary base at the 3′-end. It is shown that this additional complementary dC base and the [BP]dG residue are hydrogen bonded and that this effect induces a pronounced change in the conformation of the polycyclic aromatic pyrenyl residue at the template−primer junction of the (+)-*trans-anti*-[BP]dG·dC 13/10-mer.

**A**

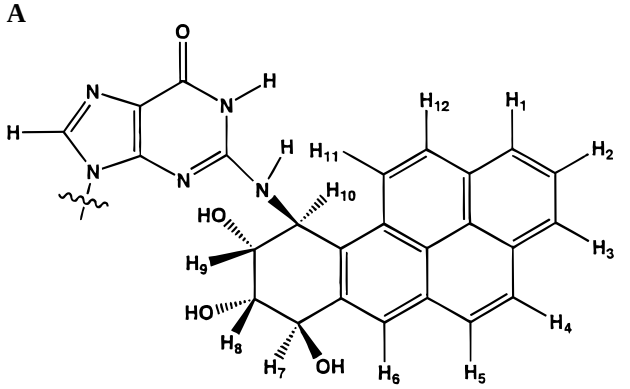


(+)-*trans-anti*-[BP]dG

**B**

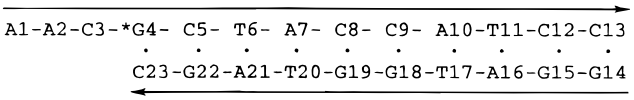


FIGURE 1: (A) Chemical structure of the (+)-*trans-anti*-[BP]dG adduct. (B) The sequence of the 13/10-mer containing the (+)-*trans-anti*-[BP]dG adduct at the *G4 position.

## MATERIALS AND METHODS

*Preparation of the (+)-trans-anti-[BP]dG·dC 13/10-Mer.* The oligodeoxynucleotides of the d(A-A-C-G-C-T-A-C-C-A-T-C-C) template and d(G-G-A-T-G-G-T-A-G-C) primer strands were synthesized on an Applied Biosystems model 392 DNA synthesizer and purified by reverse-phase HPLC. Racemic *anti*-BPDE was purchased from the National Cancer Institute Chemical Carcinogen Reference Standard Repository. The synthesis of the (+)-*trans-anti*-[BP]dG covalent adduct in the d(A-A-C-G-C-T-A-C-C-A-T-C-C) sequence was carried out starting from racemic *anti*-BPDE using previously described methods (Cosman et al., 1990). The (+)-*trans-anti*-[BP]dG containing 13-mer template strand was separable from the (−)-*trans-anti*, (−)-*cis-anti*, and (+)-*cis-anti* isomeric adducts by preparative HPLC on a C18 ODS Hypersil column (Cosman et al., 1990). The modified, enantiomerically pure d(A-A-C-[BP]G-C-T-A-C-C-A-T-C-C) 13-mer template strand was annealed to the complementary unmodified d(G-G-A-T-G-G-T-A-G-C) 10-mer primer strand at 70 °C, and the stoichiometry was followed by monitoring single proton resonances in both strands. The NMR spectra of the (+)-*trans-anti*-[BP]dG·dC 13/10-mer (Figure 1B) (approximately 8 mg) were recorded in 0.5 mL of 0.1 M NaCl, 0.01 M phosphate, and 0.1 mM $Na_2EDTA$ at pH 7.0. For observation of non-exchangeable resonances, the sample was repeatedly lyophilized and finally dissolved in 0.5 mL of 99.996% $D_2O$. For assignments of exchangeable protons, the sample was dissolved in a 9:1 $H_2O/D_2O$ buffer.

*NMR Experiments.* All experiments were recorded on Varian Unity Plus 500 and 600 MHz NMR spectrometers in the States-TPPI mode (Marion et al., 1989) with a 2 s relaxation delay between scans. A combination of through space nuclear Overhauser effect (NOESY) (Kumar et al., 1980) and through bond correlated (COSY, TOCSY) (Braumschweiler et al., 1983) spectra were recorded and analyzed to assign the carcinogen and nucleic acid protons in the (+)-*trans-anti*-[BP]dG·dC 13/10-mer. The temperature of the sample was calibrated with an external methanol sample. A

NOESY experiment with a mixing time of 100 ms was recorded on the (+)-*trans-anti*-[BP]dG·dC 13/10-mer in 90% $H_2O$/10% $D_2O$ at 1 °C using a jump and return pulse sequence. The corresponding NOESY experiments on the adduct 13/10-mer in $D_2O$ buffer were recorded as a function of mixing time at 20 °C. TOCSY experiments were recorded at spin−lock times of 40 and 80 ms in $D_2O$ buffer at 20 °C. Proton−phosphorus correlation spectra on the adduct 13/10-mer in $D_2O$ buffer, pH 7.0, at 20 °C were recorded with indirect detection (Sklenar et al., 1986). Both proton and phosphorus sweep widths were set to 6 ppm with a 1.3 s presaturation of the HDO signal. The phosphorus spectra were referenced relative to external 10% trimethyl phosphate (TMP).

Distance restraints involving non-exchangeable protons were estimated from NOE buildup curves of NOESY experiments on the adduct 13/10-mer recorded at mixing times of 50, 90, 130, 170, and 210 ms in $D_2O$ buffer. The interproton distances were calculated on the basis of the isolated two-spin approximation using the dC(H6)−dC(H5) fixed separation of 2.45 Å as the reference distance for the NOESY spectra in $D_2O$ buffer. The upper and lower bound ranges on the estimated interproton distances for non-exchangeable protons were determined on the basis of the resolution of the cross-peaks in the two-dimensional contour plots and the quality of the NOE buildup plots. The base proton to sugar H1′ NOE crosspeaks in the 50 ms mixing time NOESY data set in $D_2O$ were evaluated to qualitatively differentiate between *syn* (strong NOE) and *anti* (weak NOE) glycosidic torsion angles (Patel et al., 1987).

The proton−proton vicinal coupling constants among sugar protons were analyzed from phase-sensitive COSY and DQF-COSY spectra and used to qualitatively distinguish between the C3′-*endo* and C2′-*endo* family of sugar puckers in the (+)-*trans-anti*-[BP]dG·dC 13/10-mer. The relative intensity of the NOE crosspeaks between base protons and their own and 5′-flanking sugar H2′, H2″ and H3′ protons was used to qualitatively distinguish between the A and B family of helices for the adduct 13/10-mer (van der Ven & Hilbers, 1988). The coupling constant patterns in the benzylic ring of [BP]dG4 adduct were computed using the program CHORDS (Majumdar & Hosur, 1992) to elucidate torsion angles linking the BP(H7)−BP(H8) and BP(H9)−BP(H10) proton pairs.

*Molecular Mechanics Computations*. Molecular mechanics calculations guided by NOE distance restraints were carried out with DUPLEX (Hingerty et al., 1989) along the lines outlined in the Methods sections of previous papers from our laboratory (Cosman et al., 1993, 1994).

*Relaxation Matrix Refinement*. The final unrestrained energy minimized structure obtained during the first stage of DUPLEX calculations was used as the starting point for the second stage of refinement using X-PLOR (Brunger, 1992). During the latter stage we performed molecular dynamics/simulated annealing calculations guided by the combination of the experimental NOESY intensities and NOE distances. The pseudoenergy function included two types of restraints: (1) intensity restraints for non-exchangeable protons were imposed as square-well potentials with an exponent of 2 in the penalty function, an isotropic correlation time of 5 ns, anisotropic bounds estimates of 10%; (2) distance restraints for non-exchangeable protons were retained through our protocol as square-well potentials with uniform 20% estimation of errors and a 30 kcal/mol·Å$^2$ force constant. A 4.5 Å cutoff was imposed for computing relaxation pathways and the dynamics was carried out with a tolerance of 0.03 Å.

The relaxation matrix was set up for the non-exchangeable protons with the exchangeable imino, amino, and hydroxyl protons exchanged for deuterons. A total of 1360 non-exchangeable intensity restraints from the NOESY data sets in $D_2O$ (272 intensities per mixing time) and 270 non-exchangeable distance restraints were included in the calculations. Dihedral angle restraints (corresponding to B-DNA) were included with a very low weight of 5 kcal·rad$^{-2}$ and restricted to residues dT6−dC13 and dG14−dA21 (at least two base pairs away from [BP]dG4).

Six intensity refinement trials were performed with the starting structure in each trial heated to 1000 K through the assignment of an arbitrary Maxwell−Boltzmann velocity distribution corresponding to a temperature of 1000 K. After 2.4 ps dynamics evolution at that temperature, the system was gradually cooled to 300 K during 7.2 ps with the "heat bath" method and then equilibrated at 300 K for 2.4 ps. After equilibration the coordinates were subjected to energy minimization to a gradient of 0.1 kcal/mol·Å$^2$.

## RESULTS

*Exchangeable Nucleic Acid Proton Spectra.* The exchangeable proton NMR spectrum (11.7−14.7 ppm) of the (+)-*trans-anti*-[BP]dG·dC 13/10-mer in $H_2O$ buffer, pH 7.0 at 1 °C shows ten well-resolved imino protons between 12.4 and 14.0 ppm (Figure 2A). These imino protons have been assigned following analysis [reviewed in Patel et al. (1987) and van de Ven and Hilbers (1988)] of the 100 ms mixing time NOESY spectrum (Figure 3) of the adduct 13/10-mer at 1 °C. We can detect NOEs between adjacent imino protons from dG14 to dG22 within the helical segment of the adduct 13/10-mer (Figure 3A). We detect NOEs between the deoxyguanosine imino and deoxycytosine amino protons across all six dG·dC base pairs (peaks E−J and E′−J′, Figure 3B) and NOEs between the thymine imino and deoxyadenosine H2 protons across all four dA·dT base pairs (peaks A−D, Figure 3B) in the adduct 13/10-mer.

The imino proton of [BP]dG4 (12.81 ppm) is somewhat broader than the other imino protons (Figure 2A) and yields a broad diagonal peak in the NOESY contour plot (Figure 3A) suggestive of increased exchange kinetics with solvent water. This exchange characteristic is reflected in the weak NOEs between the imino protons of [BP]dG4 and the amino protons of dC23 (peaks E and E′, Figure 3B), which nevertheless identify formation of a Watson−Crick [BP]-dG4·dC23 junctional base pair in the adduct 13/10-mer. The imino protons of adjacent [BP]dG4 (12.81 ppm) and dG22 (12.72 ppm) are close enough to each other in chemical shift to preclude monitoring a potential NOE crosspeak between them in the NOESY contour plot (Figure 3A) of the adduct 13/10-mer. The exchangeable imino and amino proton chemical shifts for the d(A1-A2-C3-[BP]G4-C5-T6-A7)·d(T20-A21-G22-C23) segment of the (+)-*trans-anti*-[BP]-dG·dC 13/10-mer at 1 °C are listed in Table 1. The exchangeable proton chemical shifts of the entire adduct 13/10-mer are listed in Table S1 (Supporting Information).

*Non-exchangeable Nucleic Acid Proton Spectra*. The non-exchangeable base and sugar H1′ proton spectrum (5.0−8.6 ppm) of the (+)-*trans-anti*-[BP]dG·dC 13/10-mer in $D_2O$ buffer, pH 7.0 at 20 °C, is plotted in Figure 2B. The narrow

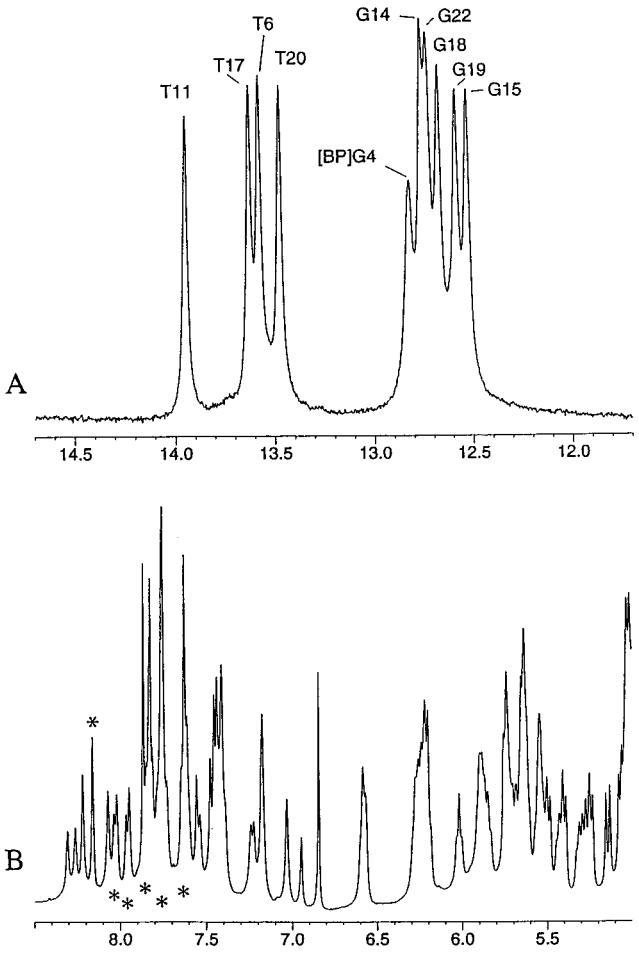


FIGURE 2: (A) Imino proton spectrum (11.7−14.7 ppm) in $H_2O$ buffer at 1 °C and (B) non-exchangeable proton spectrum (5.0−8.5 ppm) in $D_2O$ buffer at 20 °C of the (+)-*trans-anti*-[BP]dG·dC 13/10-mer. The buffer was 0.1 M NaCl and 10 mM phosphate, aqueous solution at pH 7.0. Imino proton assignments are listed over the spectrum in (A). The resolved BP resonances are designated by asterisks in (B).

Table 1: Proton Chemical Shifts of the d(A1-A2-C3-[BP]G4-C5-T6-A7)·d(T20-A21-G22-C23) of the (+)-*trans-anti*-[BP]dG·dC 13/10-mer in Aqueous Buffer

| | exchangeable proton chemical shifts (ppm), 1 °C | |
|---|---|---|
| | G(NH1)/T(NH3) | C($NH_2$-4) |
| [BP]dG4·dC23 | 12.81 | 7.02,[a] 8.29[b] |
| dC5·dG22 | 12.72 | 6.90,[a] 8.36[b] |
| dT6·dA21 | 13.57 | |
| dA7·dT20 | 13.47 | |

| | non-exchangeable proton chemical shifts (ppm), 20 °C | | | | | |
|---|---|---|---|---|---|---|
| | H8/H6 | H2/H5/$CH_3$ | H1′ | H2′,H2″ | H3′ | H4′ |
| dA1 | 7.55 | 7.87 | 5.68 | 1.48,1.85 | 4.47 | 4.01 |
| dA2 | 6.94 | 6.84 | 4.66 | 2.07,1.99 | 4.73 | 4.08 |
| dC3 | 7.73 | 5.03 | 5.32 | 1.83,2.40 | 4.78 | 3.99 |
| [BP]dG4 | 8.02 | | 6.59 | 2.99,3.11 | 4.99 | 4.50 |
| dC5 | 7.40 | 5.40 | 6.27 | 2.05,2.55 | 4.93 | 4.30 |
| dT6 | 7.40 | 1.67 | 5.53 | 2.21,2.45 | 4.91 | 4.29 |
| dA7 | 8.31 | 7.57 | 6.23 | 2.76,2.89 | 5.03 | 4.44 |
| dT20 | 7.17 | 1.33 | 5.56 | 1.97,2.29 | 4.80 | 4.10 |
| dA21 | 8.08 | 7.74 | 5.85 | 2.52,2.64 | 4.94 | 4.27 |
| dG22 | 7.48 | | 5.28 | 2.05,2.05 | 4.72 | 4.04 |
| dC23 | 6.58 | 5.07 | 3.54 | 0.15,−0.74 | 3.70 | 3.10 |

[a] Exposed amino proton. [b] Hydrogen-bonded amino proton.

and well-resolved proton resonances have permitted assignments of the non-exchangeable DNA protons in the adduct 13/10-mer. An expanded NOESY (210 ms mixing time)

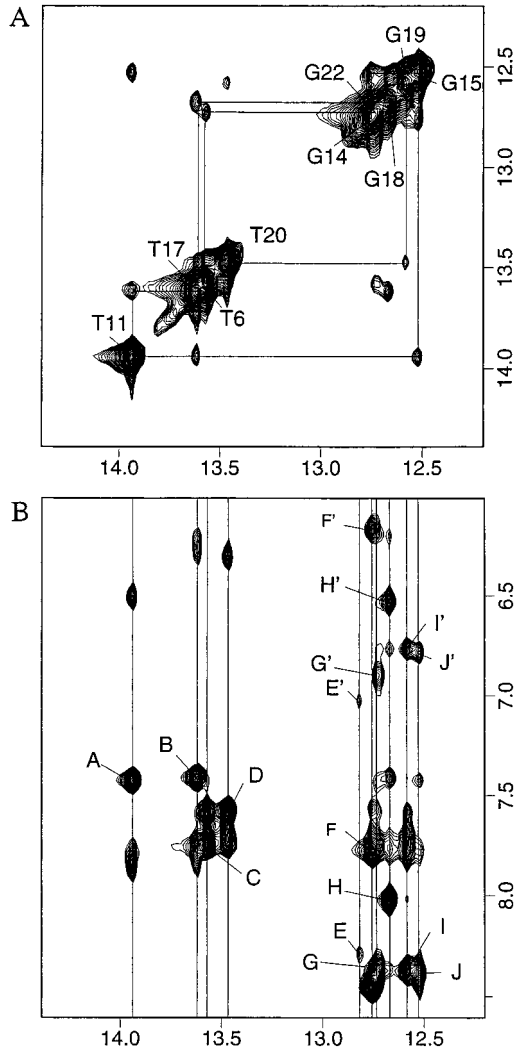


FIGURE 3: Expanded NOESY (100 ms mixing time) contour plots of the (+)-*trans-anti*-[BP]dG·dC 13/10-mer in $H_2O$ buffer at 1 °C. (A) NOE connectivities in the symmetrical 12.2−14.4 ppm region. The imino proton assignments are labeled along the diagonal. The lines trace the NOE connectivities between imino protons on adjacent base pairs starting at dG22 toward the duplex−single strand junction site and proceeding to dG14 toward the other end of the helix. (B) NOE connectivities between the imino protons (12.2−14.4 ppm) and the base and amino protons (6.0−8.6 ppm). The intramolecular crosspeaks A−J′ between nucleic acid protons are assigned as follows: (A) T11(NH3)−A16(H2); (B) T17(NH3)−A10(H2); (C) T6(NH3)−A21(H2); (D) T20(NH3)−A7(H2); (E,E′) [BP]G4(NH1)−C23($NH_2$-4a,b); (F,F′) G14(NH1)−C13($NH_2$-4a,b); (G,G′) G22(NH1)−C5($NH_2$-4a,b); (H,H′) G18(NH1)−C9($NH_2$-4a,b); (I,I′) G19(NH1)−C8($NH_2$-4a,b); (J,J′) G15(NH1)−C12($NH_2$-4a,b).

contour plot correlating the base protons (6.4−8.4 ppm) with the sugar H1′ and H3′ protons (3.0−6.7 ppm) for the adduct 13/10-mer at 20 °C is plotted in Figure 4. The NOE connectivities between the base and its own and 5′-flanking sugar H1′ protons for the d(A1-A2-C3-[BP]G4-C5-T6-A7) segment on the template strand (solid line) and the d(T20-A21-G22-C23) segment on the primer strand (dashed line) are traced in Figure 4. Distinct NOE patterns are observed for the d(A1-A2-C3-[BP]G4-C5) segment of the template strand of the adduct 13/10-mer. Thus, the NOE between adjacent residues is either absent (dC3-[BP]dG4 step), very weak (dA1-dA2 and dA2-dA3 steps) or somewhat stronger than normal ([BP]dG4-dC5 step) within this segment of the adduct 13/10-mer. Further, the base to its own H1′ protons is weaker than normal for the [BP]dG4 residue in the adduct

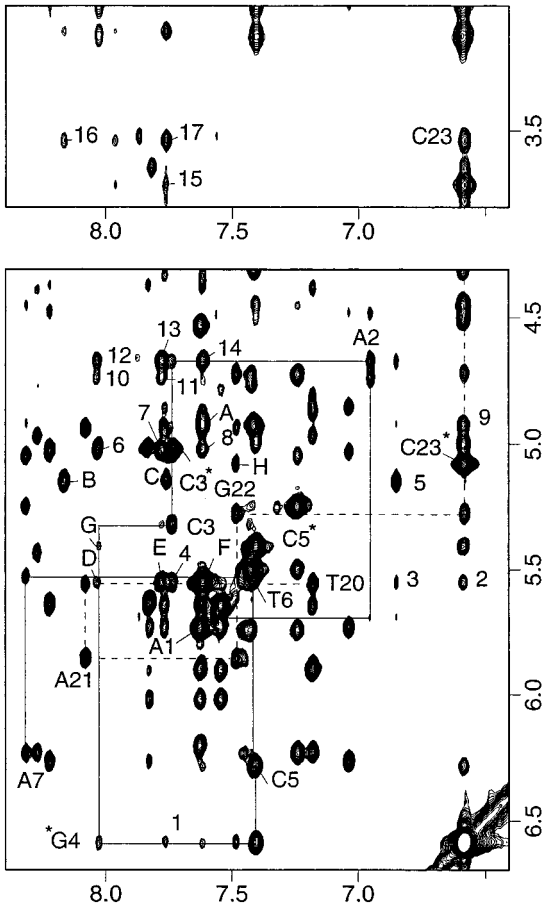


FIGURE 4: Expanded NOESY (210 ms mixing time) contour plot of the (+)-*trans-anti*-[BP]dG·dC 13/10-mer in $D_2O$ buffer at 20 °C establishing distance connectivities between the base (purine H8 and pyrimidine H6) protons (6.4−8.4 ppm) and the sugar H1′ and H3′ and deoxycytidine H5 protons (3.0−6.7 ppm). The NOE connectivities between the base and their own and 5′-flanking sugar H1′ protons from dA1 to dA7 on the template strand are shown by solid lines and from dT20 to dC23 on the primer strand are shown by dashed lines. The assignments label the base to their own sugar H1′ NOEs while the deoxycytidine H6−H5 NOEs are designated by asterisks. Note the unusual upfield shift of the H1′ proton of dC23 and the downfield shift of the H1′ proton of [BP]dG4. Note that the crosspeak linking the dC3-[BP]dG4 steps is very weak (crosspeak not detectable at the contour level in this figure) while the crosspeaks linking the dA1−dA2 and dA2−dC3 steps are weak. The intramolecular crosspeaks A−F between benzo[*a*]pyrene protons are assigned as follows: (A) BP(H9)−BP(H11); (B) BP(H6)−BP(H7); (C) BP(H5)−BP(H7); (D) BP(H1)−BP(H10); (E) BP(H10)−BP(H12); (F) BP(H11)−BP(H10). Specific intramolecular crosspeaks between DNA protons are assigned as follows: (G) [BP]G4(H8)−C5(H5); (H) G22(H8)−C23(H5). The intermolecular crosspeaks 1−17 are assigned as follows: (1) C23(H6)−BP(H4/H5); (2) [BP]G4(H1′)−BP(H10); (3) A2(H2)−BP(H10); (4) C3(H6)−BP(H10); (5) A2(H2)−BP(H7); (6) C3(H5)−BP(H1); (7) C3(H5)−BP(H12); (8) C3(H5)−BP(H11); (9) [BP]G4(H1′)−BP(H9); (10) A2(H3′)−BP(H1); (11) A2(H3′)−BP(H12); (12) A2(H1′)−BP(H1); (13) A2(H1′)−BP(H12); (14) A2(H1′)−BP(H11); (15) C23(H4′)−BP(H4/H5); (16) C23(H1′)−BP(H6); (17) C23(H1′)−BP(H4/H5). The chemical shift values for the benzylic protons are BP(H7), 5.14 ppm; BP(H8), 4.07 ppm; BP(H9), 4.92 ppm; BP(H10), 5.54 ppm. The chemical shift values for the pyrenyl protons are BP(H11), 7.61 ppm; BP(H12), 7.77 ppm; BP(H1), 8.03 ppm; BP(H2), 7.85 ppm; BP(H3), 7.96 ppm; BP(H4), 7.76 ppm; BP(H5), 7.76 ppm; BP(H6), 8.16 ppm.

13/10-mer. We also note that the base [BP]dG4 (H8) to base dC5 (H5) NOE (peak G, Figure 4) for the [BP]dG4-dC5 step is weaker than the base dG22 (H8) to base dC23 (H5) NOE (peak H, Figure 4) for the dG22−dC23 step adjacent to the junctional site in the adduct 13/10-mer.

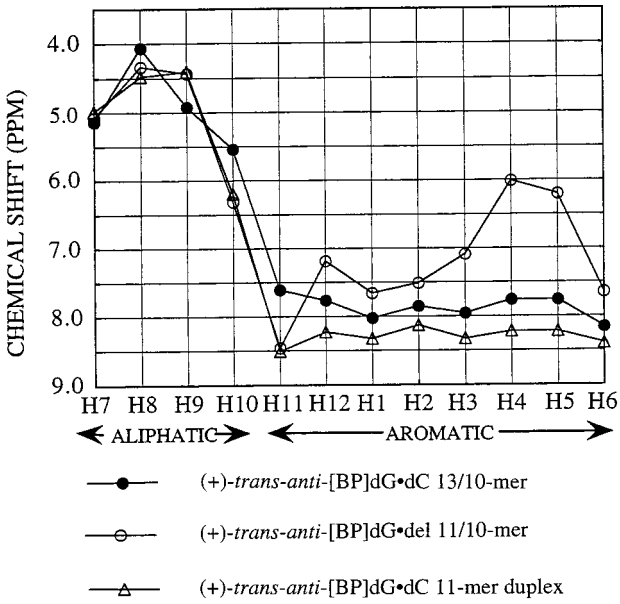


FIGURE 5: Plot comparing the benzo[*a*]pyrene ring proton chemical shifts in the (+)-*trans-anti*-[BP]dG·dC 11-mer duplex (△), the (+)-*trans-anti*-[BP]dG·del 11/10-mer (○) and the (+)-*trans-anti*-[BP]-dG·dC 13/10-mer (●). The benzylic protons (H7, H8, H9, and H10) are on the left side, and the pyrenyl protons (H11, H12, H1, H2, H3, H4, H5, and H6) are on the right side of this plot.

The non-exchangeable base and sugar proton chemical shifts have been assigned following analysis of the complete NOESY, DQF-COSY, and TOCSY data sets based on standard nucleic acid assignment procedures [reviewed in van de Ven and Hilbers (1988)]. The chemical shift values for the d(A1-A2-C3-[BP]G4-C5-T6-A7)·d(T20-A21-G22-C23) segment of the (+)-*trans-anti*-[BP]dG·dC 13/10-mer at 20 °C are listed in Table 1. The non-exchangeable proton chemical shift assignments for the entire adduct 13/10-mer are listed in Table S1 (Supporting Information).

It should be noted that several sugar proton resonances of dC23 exhibit unusual upfield chemical shifts reflecting ring current contributions from a nearby aromatic ring system. Thus, the H2′ (0.15 ppm), H2″ (−0.74 ppm), H3′ (3.70 ppm), and H4′ (3.10 ppm) sugar protons of dC23 resonate at high field (Table 1) which suggests that the pyrenyl ring of BP may stack predominantly over the sugar ring of dC23 in the adduct 13/10-mer.

*Benzo[a]pyrenyl Protons*. The benzylic and pyrenyl protons of [BP]dG4 have been assigned following analysis of the through space and through bond connectivities involving these protons in the (+)-*trans-anti*-[BP]dG·dC 13/10-mer. The chemical shifts are listed in the caption to Figure 4 and plotted in Figure 5. The chemical shifts of all aromatic pyrenyl protons resonate between 7.5−8.5 ppm in the (+)-*trans-anti*-[BP]dG·dC 13/10-mer (Figure 5).

The experimental BP(H7)−BP(H8) and BP(H9)−BP(H10) coupling crosspeaks are well resolved in the phase-sensitive COSY spectrum of the adduct 13/10-mer. We have simulated the experimental coupling crosspeak patterns and deduced three-bond vicinal proton−proton coupling constant values of $^3J$(H7,H8) = 9.6 Hz, $^3J$(H8,H9) = 2.0 Hz, and $^3J$(H9,H10) = 4.4 Hz. These coupling constants restrict the pucker of the benzylic ring to a specific distorted half-chair conformation where the BP(H7) and BP(H8) pair adopt pseudoaxial orientations while the BP(H9)−BP(H10) pair adopt pseudoequatorial conformations.

Table 2: NMR Refinement Statistics for the (+)-*trans-anti*-[BP]dG·dC 13/10-Mer

| | |
|---|---|
| NMR restraints | |
| total number of NOE intensities | 272 per mixing time |
| NOE intensities in the 6/3-mer region[a] | 145 per mixing time |
| total number of NOE distances | 270 |
| NOE distances in the 6/3-mer region[a] | 131 |
| structure statistics | |
| NMR $R_{1/6}$-factor | 0.024 ± 0.001 |
| rmsd of NOE violations | 0.047 ± 0.003 |
| number of NOE violations >0.2 Å | 3.8 ± 1.6 |
| number of NOE violations >0.2 Å in the 6/3-mer region[a] | 1.2 ± 0.4 |
| deviations from the ideal geometry | |
| bond length (Å) | 0.011 ± 0.001 |
| bond angle (deg) | 3.01 ± 0.05 |
| impropers (deg) | 0.36 ± 0.03 |
| pairwise rmsd (Å) among the six refined structures (heavy atoms only) | |
| entire 13/10-mer | 1.54 ± 0.44 |
| 6/3-mer region[a] | 1.01 ± 0.23 |
| 6/3-mer region[a] without backbone | 0.80 ± 0.31 |

[a] The d(A1-A2-C3-[BP]G4-C5-T6)·d(A21-G22-C23) segment.

*Intermolecular NOEs*. A number of intermolecular NOEs between the non-exchangeable nucleic acid protons and non-exchangeable BP protons have been identified and assigned in the NOESY spectrum of the (+)-*trans-anti*-[BP]dG·dC 13/10-mer. Several of these intermolecular NOEs are labeled in the expanded NOESY contour plot of the non-exchangeable protons in $D_2O$ solution (Figure 4) with the crosspeak assignments listed in the figure caption. These intermolecular distance restraints defined by lower and upper bounds which involve the d(A2-C3-[BP]G4-C5)·dC23 segment of the adduct 13/10-mer are listed in Table S2 (Supporting Information).

The distribution of the observed intermolecular NOEs readily identifies the orientation of the BP moiety relative to the DNA. We observe intermolecular NOEs between the benzylic H7, H9, and H10 protons and the minor groove H2 and H1′ protons of the dA2 and [BP]dG4 residues on the template strand. In addition, intermolecular NOEs are observed between the benzylic H10 proton and the major groove H5 and H6 protons of the dC3 residue on the template strand.

We observe intermolecular NOEs between the pyrenyl H11, H12, H1, H2, and H3 protons and the base and sugar protons of the dA2 residue, and the base protons of the dC3 residue on the template strand (Table S2). In addition, intermolecular NOEs are observed between the pyrenyl H1, H2, H3, and H4 protons and the sugar protons of the dC23 residue on the primer strand (Table S2). These intermolecular NOEs position the polycyclic aromatic BP ring on the 5′-side of dG4* with different edges of the pyrenyl ring interacting with the dA2−dC3 residues on the template strand and the dC23 residue on the primer strand in the adduct 13/10-mer.

*Phosphorus Spectra*. The proton decoupled phosphorus spectrum (−3.3 to −4.8 ppm) of the (+)-*trans-anti*-[BP]-dG·dC 13/10-mer in $D_2O$ at 20 °C is shown in Figure S1A (Supporting Information). The phosphorus resonances in the adduct duplex spectrum have been assigned following analysis of the proton−phosphorus correlation contour plot recorded at 20 °C (Figure S1B, Supporting Information). The most downfield-shifted phosphorus resonances are assigned to the dA2-dC3 (−3.55 ppm) and G22-C23 (−3.73 ppm) steps, while the most upfield-shifted phosphorus signal is assigned to the [BP]dG4-dC5 step (−4.66 ppm) of the (+)-*trans-anti*-[BP]dG·dC 13/10-mer.

*Molecular Mechanics Computations.* The search strategy employed in the molecular mechanics calculations began with an energy-minimized B-DNA (Arnott et al., 1976) d(A1-A2−C3-[BP]G4-C5-T6)·d(A21-G22-C23) 6/3-mer segment from the (+)-*trans-anti*-[BP]dG·dC 13/10-mer. The benzylic ring was fixed in the distorted half-chair conformation with BP(H9) and BP(H10) in pseudoequatorial orientations while BP(H7) and BP(H8) were in the pseudoaxial orientations (Neidle et al., 1982), as defined by the coupling constant data on the adduct 13/10-mer. The BP-DNA orientation space was then searched with sixteen energy minimization trials. In these trials, the linkage torsional angles α′ ([BP]-dG4($N^1$)-[BP]dG4($C^2$)-[BP]dG4($N^2$)-BP($C^{10}$)) and β′ ([BP]-dG4($C^2$)-([BP]dG4($N^2$)-BP($C^{10}$)-BP($C^9$)) were each started at 0°, 90°, 180°, and 270° in all combinations. The computations were guided by the NMR-based distance restraints defined by lower and upper bounds which are listed in Table S2 (Supporting Information).

A superpositioned view of the d(A1-A2-C3-[BP]G4-C5-T6)·d(A21-G22-C23) segment of the three lowest energy computed conformations (superpositioned on the helical segments) is plotted in Figure S2 (Supporting Information). The d(A1-A2-C3-[BP]G4-C5-T6)·d(A21-G22-C23) segment of the lowest energy structure was next employed in building the (+)-*trans-anti*-[BP]dG·dC 13/10-mer. Subsequently, the hydrogen-bond penalty function and the distance restraints were released with energy minimization, yielding an unrestrained minimum energy conformation of the (+)-*trans-anti*-[BP]dG·dC 13/10-mer (Figure S3, Supporting Information). This structure was then employed in the second stage relaxation matrix refinement calculations as described in Materials and Methods.

*Relaxation Matrix Refinement.* An ensemble of six structures obtained during intensity refinement demonstrated an improved correspondence with experimental intensity and distance restraint data sets. The number of NOE distances violated by more than 0.2 Å decreased from 18 to 4 (with one or no violations in the d(A1-A2-C3-[BP]G4-C5-T6)·d(A21-G22-C23) segment with respect to different structures in the ensemble), and the NMR $R_{1/6}$-factor improved from an initial value of 8% to 2% (Table 2). The structures exhibit good stereochemistry with rmsd values for bond length, bond angle and improper dihedral angle violations of 0.011 ± 0.001 Å, 3.01 ± 0.05°, and 0.36 ± 0.03°, respectively (Table 2).

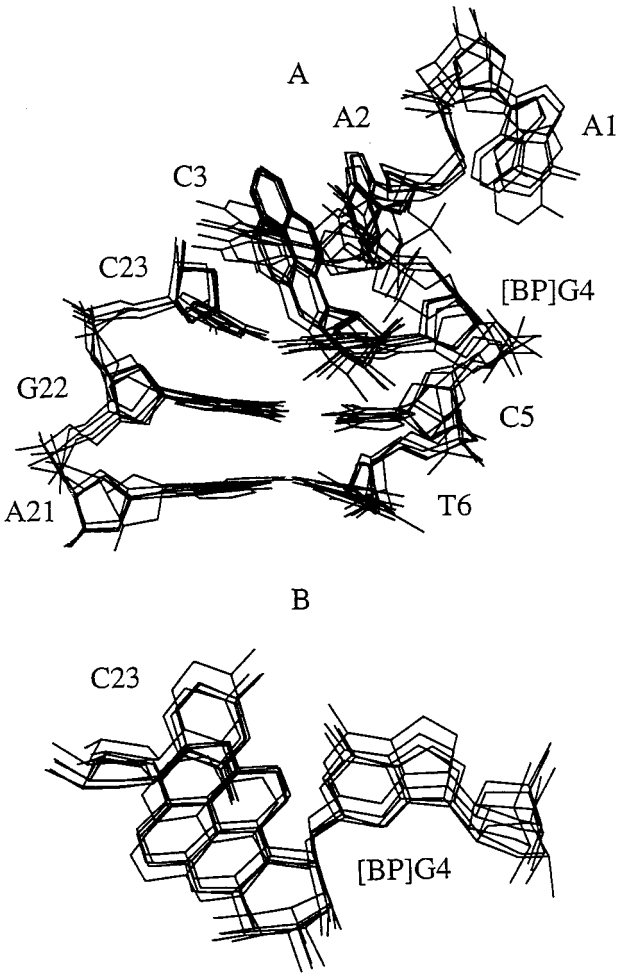


FIGURE 6: (A) Superposition of the d(A1-A2-C3-[BP]G4-C5-T6)·d(A21-G22-C23) segment of the six relaxation matrix refined structures of the (+)-*trans-anti*-[BP]dG·dC 13/10-mer. View looking into the minor groove and normal to the helix axis of the central segments. (B) Superposition of the [BP]dG4·dC23 base pair of the six relaxation matrix refined structures of the (+)-*trans-anti*-[BP]-dG·dC 13/10-mer. View looking down the helix axis.

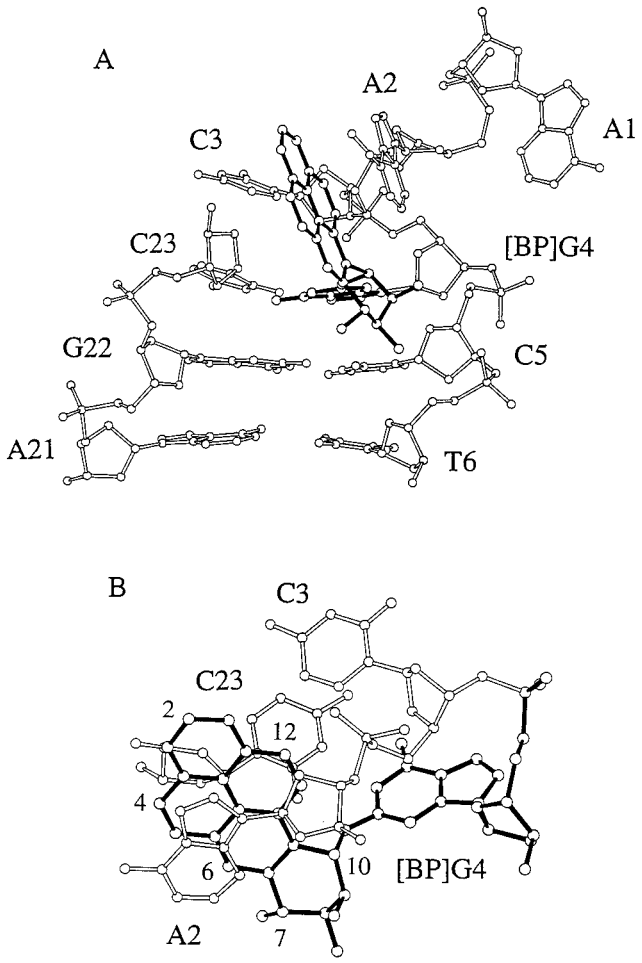


FIGURE 7: The representative structure of the (+)-*trans-anti*-[BP]-dG·dC 13/10-mer from the ensemble of six relaxation matrix refined structures. (A) View looking into the minor groove and normal to the helix axis for the d(A1-A2-C3-[BP]G4-C5-T6)·d(A21-G22-C23) segment. (B) View looking down the helix axis for the d(A2-C3-[BP]G4)·dC23 segment. The benzylic ring is positioned in the minor groove while the pyrenyl ring stacks over the sugar ring of dC23 and points toward the 5′-end of the template strand.

The rmsd values of all heavy atoms between the six structures and the initial structure is 2.48 ± 0.11 Å for all heavy atoms and 2.95 ± 0.21 Å for the d(A1-A2-C3-[BP]-G4-C5-T6)·d(A21−G22-C23) segment. At the same time the convergence among the structures themselves was excellent. The pairwise rmsd in the set is 1.54 ± 0.44 Å for all heavy atoms, 1.17 ± 0.1 Å for the heavy atoms of the d(A1-A2-C3-[BP]G4-C5-T6)·d(A21-G22-C23) segment, and 0.80 ± 0.31 Å for the heavy atoms of the d(A1-A2-C3-[BP]G4-C5-T6)·d(A21-G22-C23) segment excluding backbone (Table 2).

The corresponding superpositioned view of the six conformations of the d(A1-A2-C3−[BP]G4-C5-T6)·d(A21-G22-C23) segment is plotted in Figure 6A. A view looking down the helix axis of the [BP]dG4·dC23 base pair in the six superpositioned conformations is plotted in Figure 6B.

*Solution Structure*. A view normal to the helix axis and looking into the minor groove for the d(A1-A2-C3-[BP]G4-C5-T6)·d(A21-G22-C23) segment of the representative structure from the ensemble of six relaxation matrix refined structures of the (+)-*trans-anti*-[BP]dG·dC 13/10-mer is shown in Figure 7A. The covalently linked BP moiety is located on the minor groove side of the modified dG4 residue, while the [BP]dG4 maintains Watson−Crick hydrogen bonding with its partner dC23 base (Figure 7A). This orientation of the polycyclic aromatic BP ring system in the template−primer junction is reminiscent of the minor groove conformation observed for the stereochemically identical lesion in a full base-paired B-DNA duplex (Cosman et al., 1992). A view looking down the helix axis of the d(A2-C3-[BP]G4)·dC23 segment of the solution structure of the (+)-*trans-anti*-[BP]dG·dC 13/10-mer is shown in Figure 7B, which emphasizes the overlap geometry between the pyrenyl ring system and the A2 base and C23 sugar, and the alignment of the BP ring system relative to the modified base dG4. The pyrenyl ring system of the BP moiety stacks over the sugar ring of the dC23 partner residue, with the $C^{11}$-$C^{12}$-$C^{1}$-$C^{2}$ long edge of the BP ring directed toward the major groove side of dC23, and the $C^{4}$-$C^{5}$-$C^{6}$-containing long edge of the BP ring directed toward the minor groove side (Figure 7B). The dC3 base is displaced into the major groove, allowing dA2 positioned in the minor groove to stack over the pyrenyl ring of the BP moiety in the adduct 13/10-mer (Figure 7B). The benzylic ring of BP is in a distorted half-chair conformation with the BP(H9) and BP(H10) in pseudoequatorial orientations while BP(H7) and BP(H8) adopt pseudoaxial orientations. The carcinogen-base linkage site for the [BP]dG4 residue is defined by the angles $\alpha'$ [dG4-($N^{1}$)-dG4($C^{2}$)-dG4($N^{2}$)-BP($C^{10}$)] = 196 ± 2° and $\beta'$ [dG4-($C^{2}$)-dG4($N^{2}$)-BP($C^{10}$)-BP($C^{9}$)] = 278 ± 6° among the

ensemble of six structures obtained from the relaxation matrix refinement of the (+)-*trans-anti*-[BP]dG·dC 13/10-mer.

Some of the glycosidic torsion angles and sugar puckers for the d(A2-C3-[BP]G4-C5-T6)·d(A21-G22-C23) segment of the (+)-*trans-anti*-[BP]dG·dC 13/10-mer differ from those most common in B-DNA duplexes (Berman et al., 1992). The ensemble of six structures obtained from the relaxation matrix refinement was B-like except that the glycosidic torsion angle $\chi$ for dC3, which is in the *anti* range but adopts an unusual low value of 149.5 ± 4.6°. For [BP]dG4, $\chi$ is 268.8 ± 19.9° and is in the *anti* range. The pseudorotation *P* value of dC23 is 48.2 ± 2.2°, thus places this sugar in the C3′-*endo* domain.

## DISCUSSION

*Spectral Quality and Information Content.* The (+)-*trans-anti*-[BP]dG·dC 13/10-mer adopts a single conformation based on the well-resolved exchangeable imino (Figure 2A) and non-exchangeable (Figure 2B) proton spectra. The exchangeable and non-exchangeable protons are narrower and better resolved for the (+)-*trans-anti*-[BP]dG·dC 13/10-mer containing the junctional [BP]dG adduct opposite dC (this study) compared to the corresponding proton spectra for the (+)-*trans-anti*-[BP]dG 13/9-mer lacking a base opposite the junctional [BP]dG adduct (Cosman et al., 1995).

*NOE Patterns.* The combined NMR-computational studies establish that the BP ring system of the (+)-*trans-anti*-[BP]dG·dC 13/10-mer is tilted toward the 5′-end of the modified strand; this orientation has features similar to the minor groove conformation adopted by the stereochemically identical (+)-*trans-anti*-[BP]dG lesion opposite dC in the full 11-mer duplex (Cosman et al., 1992). The duplex segment located 3′ to the modified guanine adopts an unperturbed B-DNA conformation with all ten base pairs, including the [BP]dG4·dC23 junctional pair at the modification site, retaining Waston-Crick alignment in the adduct 13/10-mer. The dA2 and dC3 residues of the single strand segment are displaced toward the minor and major grooves, respectively, with loss of stacking between neighbors within the d(A2-C3-[BP]G4) segment in the adduct 13/10-mer. The glycosidic torsion angle of the modified guanine is within the *anti* range consistent with its participation in a Watson−Crick [BP]dG4·dC23 alignment in the adduct 13/10-mer.

The alignment of the pyrenyl ring system toward the minor groove side of the [BP]dG4, directed toward the 5′-end of the template strand and stacked directly over the A2 base and C23 sugar rings in the solution structure of the (+)-*trans-anti*-[BP]dG·dC 13/10-mer (Figure 7), is strongly supported by the experimental NOE patterns. The orientation of the BP ring system toward the 5′-end of the modified strand (Figure 7B) results in the observation of intermolecular NOEs between the BP(H11), BP(H12), BP(H1) and BP(H2) protons and base and sugar protons of dA2 and dC3 in the adduct 13/10-mer (Table S2). The stacking of the BP ring over the sugar residue of dC23 (Figure 7B) results in a number of additional NOEs between the BP(H1), BP(H2), BP(H3) and BP(H4) protons and the sugar protons of dC23 in the adduct 13/10-mer (Table S2).

*Chemical Shift Patterns*. The stacking interactions between the aromatic pyrenyl ring system in the (+)-*trans-anti*-[BP]dG·dC 13/10-mer and the dC23 sugar ring in one direction and the dA2 base in the opposite direction are also evident from the pronounced upfield chemical shift changes observed for the sugar protons of dC23 and the base protons of dA2. Experimentally, large upfield shifts are detected at the H1′ (−2.53 ppm), H2′ (−1.94 ppm), H2″ (−2.91 ppm), H3′ (−0.76 ppm), and H4′ (−0.93 ppm) protons of dC23, as well as the H8 (−1.18 ppm) proton of dA2 on proceeding from the control dG·dC 13/10-mer to the [BP]dG·dC 13/10-mer (Table S3, Supporting Information).

The aromatic pyrenyl protons in the (+)-*trans-anti*-[BP]-dG·dC 13/10-mer exhibit chemical shift values between 7.5−8.5 ppm, which are comparable to the values for analogous protons in the solvent-exposed minor groove structure of the (+)-*trans-anti*-[BP]dG·dC 11-mer duplex (Cosman et al., 1992) as shown in Figure 5.

*Comparison of First-Stage DUPLEX and Second-Stage X-PLOR Intensity Refined Structures.* The key conformational features centered about the [BP]dG adduct site are shared by both the first-stage DUPLEX and second-stage X-PLOR intensity refined structures of the (+)-*trans-anti*-[BP]dG 13/10-mer. This includes the Watson−Crick alignment of the [BP]dG4·dC23 base pair and the relative alignment of the 5′-oriented pyrenyl ring in the minor groove where it stacks over the dA2 base ring in one direction and the dC23 sugar ring in the opposite direction. Further, the carcinogen−base linkage site torsion angles $\alpha'$ [dG4($N^1$)-dG4($C^2$)-dG4($N^2$)-BP($C^{10}$)] and $\beta'$ [dG4($C^2$)-dG4($N^2$)-BP($C^{10}$)-BP($C^9$)] are 222° and 276°, respectively, for the lowest energy DUPLEX derived structure and are 196 ± 2° and 278 ± 6°, respectively, for the X-PLOR intensity refined structures. The discussion presented below will use the relaxation matrix refined structure of the (+)-*trans-anti*-[BP]-dG 13/10-mer for comparison with related DUPLEX-based structures of (+)-*trans-anti*-[BP]dG 13/9-mer (Cosman et al., 1995), (+)-*trans-anti*-[BP]dG·dC 11-mer duplex (Cosman et al., 1992) and (+)-*trans-anti*-[BP]dG·del 11/10-mer (Cosman et al., 1994) published previously.

*Differences in the Conformations of the (+)-trans-anti-[BP]dG·dC 13/10-Mer and the (+)-trans-anti-[BP]dG 13/9-Mer*. The solution structures of the first six bases starting from the 5′-end of the modified strand and the associated complementary bases, the 6/3-mer segment of the (+)-*trans-anti*-[BP]dG 13/10-mer (this study) and the 6/2-mer segment of the (+)-*trans-anti*-[BP]dG 13/9-mer (Cosman et al., 1995), are compared to one another in the same relative global orientation of the DNA in Figures 8A and 8B, respectively. We note that the orientation of the [BP]dG residues are strikingly different in these two structures that differ in whether a dC residue is present (13/10−mer) or absent (13/9-mer) opposite the junctional [BP]dG adduct. The benzo[*a*]pyrenyl ring stacks over the adjacent junctional dC5·dG22 base pair located on the duplex segment proximate to the modified deoxyguanosine in the adduct 13/9-mer (Figure 8B). Furthermore, the modified deoxyguanosine residue adopts a *syn* glycosidic torsion angle and is displaced toward the major groove side in the adduct 13/9-mer (Figure 8B). By contrast, the benzo[*a*]pyrenyl ring is positioned on the minor groove side of the [BP]dG4 moiety and oriented toward the 5′-end of the modified strand in the adduct 13/10-mer (Figure 8A). Furthermore, the modified dG4 residue maintains Watson−Crick base pairing with the partner dC23 and adopts an *anti* glycosidic torsion angle in the adduct 13/10-mer (Figure 8A). Thus, adding the partner base dC23 opposite the (+)-*trans-anti*-[BP]dG lesion at the junction site results in a dramatic conformational transition in the adduct

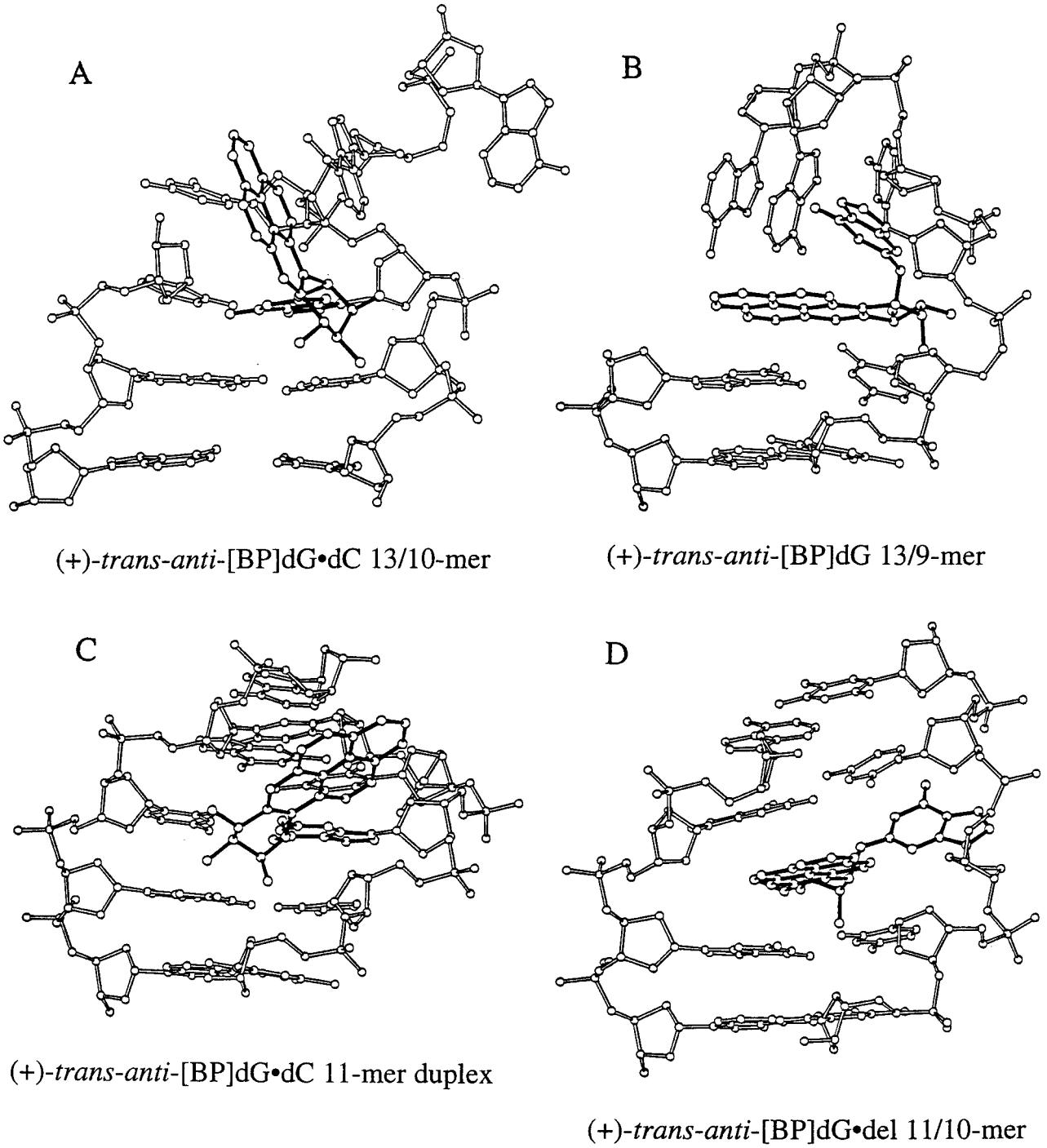


FIGURE 8: Views looking into the minor groove and normal to the helix axis for the solution structures of (A) the 6/3-mer d(A1-A2-C3-[BP]G4-C5-T6)·d(A21-G22-C23) segment of the (+)-*trans-anti*-[BP]dG·dC 13/10-mer following relaxation matrix refinement (this study), (B) the 6/2−mer d(A1-A2-C3-[BP]G4-C5-T6)·d(A21-G22) segment of the (+)-*trans-anti*-[BP]dG 13/9-mer following DUPLEX refinement (Cosman et al., 1995), (C) the 5/5-mer d(T4-C5-[BP]G6-C7-T8)·d(A15-G16-C17-G18-A19) segment of the (+)-*trans-anti*-[BP]dG·dC 11-mer duplex following DUPLEX refinement (Cosman et al., 1992), and (D) the 5/4-mer d(T4-C5-[BP]G6-C7-T8)·d(A15-G16-G17-A18) segment of the (+)-*trans-anti*-[BP]dG·del 11/10-mer following DUPLEX refinement (Cosman et al., 1994).

13/10-mer since the polycyclic aromatic BP residue no longer stacks over the adjacent dC5·dG22 base pair as it does in the adduct 13/9-mer that lacks the dC23 base.

*Comparison of the (+)-trans-anti-[BP]dG·dC 13/10-Mer and the (+)-trans-anti-[BP]dG·dC 11-Mer Duplex.* The solution structures of the 6/3-mer segment of the (+)-*trans-anti*-[BP]dG·dC 13/10-mer (this study) and the 5/5-mer segment of the (+)-*trans-anti*-[BP]dG·dC 11-mer duplex (Cosman et al., 1992) are compared in Figures 8A and 8C, respectively. These two modified sequences with stereochemically identical (+)-*trans-anti*-[BP]dG lesions opposite dC positioned either in junctional or duplex contexts share some common structural features centered about the lesion site. These include the relative orientations of the BP moieties toward the 5′-side of the modified strand in the minor groove of the adduct 11-mer duplex (Figure 8C) and a similar orientation toward the 5′-side of the dG4·dC23 base pair in the adduct 13/10-mer (Figure 8A). However, the solution structure of the (+)-*trans-anti*-[BP]dG·dC 13/10-mer differs from that of the (+)-*trans-anti*-[BP]dG·dC 11-mer duplex in that the benzo[*a*]pyrenyl ring stacks over the sugar ring of the dC residue positioned opposite it in the adduct 13/10-mer (Figure 8A), whereas the BP ring stacks over the sugar-phosphate backbone of the partner strand

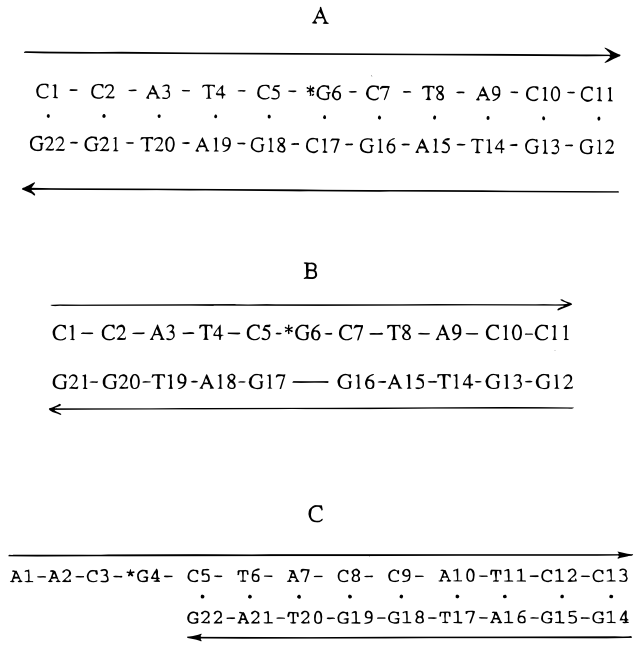


FIGURE 9: The sequences of (A) the [BP]dG·dC 11-mer duplex, (B) the [BP]dG·del 11/10-mer, and (C) the [BP]dG 13/9-mer.

toward the 5′-side of the modified dG residue in the solution structure of the adduct 11-mer duplex (Figure 8C).

*Different Conformations of (+)-trans-anti-[BP]dG·dC 13/10-Mer and (+)-trans-anti-[BP]dG·del 11/10-Mer.* The remarkable variations in the conformations of the (+)-*trans-anti*-[BP]-$N^2$-dG lesions in different sequence contexts is further illustrated by comparing the solution structures of the 6/3-mer segment of the (+)-*trans-anti*-[BP]dG·dC 13/10-mer (this study) and the central 5/4-mer segment of the (+)-*trans-anti*-[BP]dG·del 11/10-mer (Cosman et al., 1994) shown in Figures 8A and 8D, respectively. The sequence of the (+)-*trans-anti*-[BP]dG·del 11/10-mer is identical to that of the fully complementary 11-mer duplex (Cosman et al., 1992) except that the partner dC base opposite the [BP]-dG residue is missing (−1 deletion duplex). The benzo[*a*]-pyrenyl ring intercalates between the flanking dG·dC base pairs by displacing the modified deoxyguanosine into the major groove, where it stacks over the major groove face of the 5′-flanking deoxycytosine in the structure of the (+)-*trans-anti*-[BP]dG·del 11/10-mer (Figure 8D).

*Effects of Local Base Sequence Context on the Conformations of the (+)-trans-anti-[BP]dG Lesions.* A comparison of the conformations of the (+)-*trans-anti*-[BP]dG lesions in the junctional adduct 13/10-mer (Figure 8A) (this study), the junctional adduct 13/9-mer (Figure 8B) (Cosman et al., 1995), the adduct 11/10-mer deletion duplex (Figure 8D) (Cosman et al., 1994) and the fully complementary 11-mer duplex (Figure 8C) (Cosman et al., 1992), indicates that the structural features of the benzo[*a*]pyrenyl residues are remarkably dependent on the presence or absence of the partner base dC opposite the [BP]dG modified adduct site, as well as on whether the adduct is positioned within a duplex or at a template−primer junctional site.

The possibility of hydrogen bonding of the modified dG with a dC residue on the complementary strand, as well as stacking interactions between the hydrophobic aromatic BP residue and neighboring DNA bases, appear to be strong determinants of the (+)-*trans-anti*-[BP]dG lesion conformations. In the fully complementary adduct 11-mer duplex, the polycyclic aromatic BP residue is positioned within the minor groove on the 5′-side of the modified dG residue with one face exposed to the aqueous solvent environment (Figure 8C) (Cosman et al., 1992). In the absence of the dC residue in the partner strand opposite the lesion, the hydrophobic BP residue is no longer situated in the partially solvent-exposed minor groove but is inserted between two adjacent dG·dC base pairs into a hydrophobic intercalation site created by displacement of the modified dG residue, in the adduct 11/10-mer deletion duplex (Figure 8D) (Cosman et al., 1994). Similarly, in the junctional adduct 13/9-mer sequence in which the partner dC base is missing, flexibility in the torsional angles $\alpha'$, $\beta'$, and $\chi$ allow for stacking of the aromatic BP residue with the dC5·dG22 base pair adjacent to the lesion on its 3′-side; in this conformation, one face of the stacked hydrophobic BP residue avoids exposure to the aqueous solvent environment (Figure 8B) (Cosman et al., 1995). However, in the junctional adduct 13/10-mer, the presence of the dC23 residue opposite the lesion permits hydrogen bonding with the modified dG4 residue; the aromatic BP ring system is now tilted away from the dC5·dG22 base pair and assumes a conformation (Figure 8A) (this study) that has features similar to the minor groove structure in the fully complementary adduct 11-mer duplex (Figure 8C) (Cosman et al., 1992). However, the values of $\alpha'$ in the adduct 11/10-mer deletion duplex and the junctional adduct 13/10-mer structures deviate in opposite directions from the value of $\alpha' = 180°$ which defines perfect hydrogen bonding in the fully complementary adduct 11-mer duplex (Geacintov et al., 1997); in the adduct 11/10-mer deletion duplex $\alpha' = 137°$ while in the junctional adduct 13/10-mer sequence $\alpha' = 222°$. Such a difference may allow for a better interaction of the BP ring system with the single-stranded segment of the junctional adduct 13/10−mer.

*Biological Implications.* When [BP]dG is positioned at a primer-template junction with no partner opposite the lesion (13/9-mer), the BP modified dG is in the *syn* conformation and is thus positioned abnormally at the DNA replication junction; furthermore, the pyrenyl residue is stacked with the junctional dG·dC base pair (Cosman et al., 1995). When the length of the primer strand is extended by a single base with a dC positioned opposite the lesion site (13/10-mer, this work), the orientation of the BP residue is strikingly different since it is now directed toward the 5′-end of the modified strand. Although it is not identical to the duplex structure, the adduct conformation in our 13/10−mer primer−template model system resembles the minor groove structure reported for full duplexes (Cosman et al., 1992; Fountain & Krugh, 1995).

These adduct conformations, if they continue to be relevant in complexes with polymerases during DNA replication, are expected to hinder the insertion of the 2′-deoxynucleotide triphosphates (dNTP) opposite the modified bases, as observed experimentally in primer extension reactions *in vitro* (Hruszkewycz et al., 1992; Shibutani et al., 1993; Geacintov et al., 1997). However, primer extension by a single base by insertion of a single dNTP opposite the base flanking the lesion on the 3′-side on the template strand should be much less hindered. These predictions have been verified experimentally in site-specific, single base primer extension reactions catalyzed by *Pol*I (Klenow fragment, exo-) in the immediate vicinity of the (+)-*trans-anti*-[BP]dG lesion in 13/8-mer, 13/9-mer and 13/10-mer template−primer complexes of the same sequence as studied in this work (Shibutani et al., 1993; Li, 1995). The mutagenic potentials

of this lesion *in vivo* in different sequence contexts have also been investigated (Mackay et al., 1992; Jelinsky et al., 1995; Moriya et al., 1996). However, the relationships between adduct conformation, mutagenic specificity and the effects of neighboring bases on the observed mutation frequencies and spectra remain to be elucidated (Jelinsky et al., 1995; Moriya et al., 1996).

In summary, a subtle interplay between hydrogen bonding effects involving the modified dG base and dC residue on the partner strand on the one hand, and carcinogen−DNA base stacking/intercalation interactions on the other, determines whether minor groove-like or carcinogen−base stacked/intercalated adduct conformations are dominant. While the important question associated with the effect of enzymes on the conformations and biological consequences of these lesions remains to be resolved in the future, the present 13/10-mer structure and the previously studied 13/9-mer structure (Cosman et al., 1995) constitute important steps in characterizing the nature of the interactions at BP-modified primer−template junctions. It is likely that in a ternary DNA polymerase−(template−primer)−dNTP complex, the nature of the interactions between the polycyclic aromatic ring system and the enzymes as well as the noncovalently bound deoxynucleotide triphosphates can strongly influence polymerase stalling, normal primer extension, or the insertion of an incorrect base into the growing primer strand.

*Coordinate Deposition.* The coordinates of the (+)-*trans-anti*-[BP]dG·dC 13/10-mer are being deposited in the Protein Data Base, Brookhaven National Laboratory, Upton, New York 11923, from whom copies can be obtained (accession code, 1AXO).

## SUPPORTING INFORMATION AVAILABLE

Three tables listing exchangeable and non-exchangeable proton chemical shifts for the entire (+)-*trans-anti*-[BP]dG·dC 13/10-mer, a comparison of experimental intermolecular distance restraints with their relaxation matrix refined computed counterparts and proton chemical shift differences on adduct formation, and three figures showing the phosphorus spectra, the superposition of three structures that best fit the NMR data obtained by molecular mechanics calculations using DUPLEX, and the final unrestrained energy minimized structure obtained by molecular mechanics calculations using Duplex (9 pages). Ordering information is given on any current masthead page.

## REFERENCES


Altona, C., & Sundaralingam, M. (1972) *J. Am. Chem. Soc. 94*, 8205−8212.

Arnott, S., Bond, P. J., Selsing, E., & Smith, P. J. (1976) *Nucleic Acids Res. 3*, 2459−2470.

Berman, H. M., Olson, W. K., Beveridge, D. L., Westbrook, J., Gelbin, A., Demeny, T., Hsieh, S. H.., Srinavasan, A. R., & Schneider, B. (1992) *Biophys. J. 63*, 751−759.

Braumschweiler, L., Ernst, R. R., & Wuthrich, K. (1983) *J. Magn. Reson. 53*, 521−528.

Brunger, A. T. (1992) *X-PLOR User Manual*, version 3.1, Yale University, New Haven, CT.

Cosman, M., Ibanez, V., Geacintov, N. E., & Harvey, R. G. (1990) *Carcinogenesis 11*, 1667−1672.

Cosman, M., de los Santos, C., Fiala, R., Hingerty, B. E., Singh, S., Ibanez, V., Margulis, L., Live, D., Geacintov, N. E., Broyde, S., & Patel, D. J. (1992) *Proc. Natl. Acad. Sci. 89*, 1914−1918.

Cosman, M., de los Santos, C., Fiala, R., Hingerty, B. E., Ibanez, V., Luna, E., Harvey, R. G., Geacintov, N. E., Broyde, S., & Patel, D. J. (1993) *Biochemistry 32*, 4145−4155.

Cosman, M., Fiala, R., Hingerty, B. E., Amin, S., Geacintov, N. E., Broyde, S., & Patel, D. J. (1994) *Biochemistry 33*, 11507−11517.

Cosman, M., Hingerty, B. E., Geacintov, N. E., Broyde, S., & Patel, D. J. (1995) *Biochemistry 34*, 15334−15350.

Cosman, M., Hingerty, B. E., Luneva, N., Amin, S., Geacintov, N. E., Broyde, S., & Patel, D. J. (1996) *Biochemistry 35*, 9850−9863.

de los Santos, C., Cosman, M., Hingerty, B. E., Ibanez, V., Margulis, L., Geacintov, N. E., Broyde, S., & Patel, D. J. (1992) *Biochemistry 31*, 5245−5252.

Denissenko, M. F., Pao, A., Tang, M.-S., & Pfeifer, G. (1996) *Science 274*, 430−432.

Fountain, M. A., & Krugh, T. R. (1995) *Biochemistry 34*, 3152−3161.

Geacintov, N. E., Cosman, M., Mao,B., Alfano, A., Ibanez, V., & Harvey, R. G. (1991) *Carcinogenesis 12*, 2099−2108.

Geacintov, N. E., Cosman, M., Hingerty, B. E., Amin, S., Broyde, S., & Patel, D. J. (1997) *Chem. Res. Toxicol. 10*, 111−146.

Greenblatt, M. S., Bennett, W. P., Hollstein, M., & Harris, C. C. (1994) *Cancer Res. 54*, 4855−4878.

Harvey, R. G., *Polycyclic Aromatic Hydrocarbons: Chemistry and Carcinogenicity*, Cambridge University Press, Cambridge, U.K., 1991.

Hingerty, B. E., & Broyde, S. (1985) *Biopolymers 24*, 2279−2299.

Hingerty, B. E., Figueroa, S., Hayden, T., & Broyde, S. (1989) *Biopolymers 28*, 1195−1222.

Hruszkewycz, A. M.,Canella, K. A., Peltonen, K., Kotrappa, L., & Dipple, A. (1992) *Carcinogenesis 13*, 2347−2352.

Jelinsky, S. A., Liu, T., Geacintov, N. E., & Loechler, E. L. (1995) *Biochemistry 34*, 13545−13553.

Kumar, A, Ernst, R. R., & Wuthrich, K. (1980) *Biochem. Biophys. Res. Commun. 95*, 1−6.

Li, B. (1995) Ph.D. Thesis, New York University, New York.

Mackay, W., Benasutti, M., Drouin, E., & Loechler, E. L. (1992) *Carcinogenesis 13*, 1415−1425.

Majumdar, A., & Hosur, R. V. (1992) *Prog. in NMR Spectrosc. 24*, 109−158.

Marion, D., Ikura, M., Tschudin, R., & Bax, A. (1989) *J. Magn. Reson. 85*, 393−399.

Moriya, M., Spiegel, S., Fernandes, A., Amin, S., Liu, T.-M., Geacintov, N. E., & Grollman, A. P. (1996) *Biochemistry 35*, 16646−16656.

Neidle, S., Subiah, A., Kuroda, R., & Cooper, C. S. (1982) *Cancer Res. 42*, 3716−3768.

Patel, D. J., Shapiro, L., & Hare, D. (1987) *Annu. Rev. Biophys. Biophys. Chem. 16*, 423−454.

Pontén, I., Kim, S. K., Gräslund, A., Nordén, B., & Jernström, B. (1994) *Carcinogenesis 15*, 2207−2213.

Reardon, D. B., Bigger, A. C. H., Strandberg, J., Yagi, H., Jerina, D. M., & Dipple, A. (1989) *Chem. Res. Toxicol. 2*, 12−14.

Rodriguez, H., & Loechler, E. L. (1993) *Biochemistry 32*, 1759−1769.

Ross, J. A., Nelson, G. B., Wilson, K. H., Rabinowitz, J. R., Galati, A., Stoner, G. D., Nesnow, S., & Mass, M. J. (1995) *Cancer Res. 55*, 1039−1044.

Shibutani, S., Margulis, L. A., Geacintov, N. E., & Grollman, A. P. (1993) *Biochemistry 32*, 7531−7541.

Singer, B., & Grunberger, D. (1983) *Molecular Biology of Mutagens and Carcinogens*, Plenum Press, New York.

Sklenar, V., Miyashiro, H., Zon, G., Miles, H. T., & Bax, A. (1986) *FEBS Lett. 208*, 94−98.

Suh, M., Ariese, F., Small, G. J., Jankowiak, R., Liu, T.-M., & Geacintov, N. E. (1995) *Biophys. Chem. 56*, 281−296.

van der Ven, F. J., & Hilbers, C. W. (1988) *Eur. J. Biochem. 178*, 1−38.

Wei, S. J. C., Chang, R. L., Wong, C.-Q., Bhachech, N., Cui, X. X., Hennig, E., Yagi, H., Sayer, J. M., Jerina, D. M., Preston, B. D., & Conney, A. H. (1991) *Proc. Natl. Acad. Sci. U.S.A. 88*, 11227−11230.

Zou, Y., Liu, T.-M., Geacintov, N. E., & Houten, B. V. (1995) *Biochemistry 34*, 13582−13593.


BI970069S